
# Automatic Macular Edema Identification and Characterization Using OCT Images

Gabriela Samagaio, AiAda Estévez, Joaquim de Moura, Jorge Novo, Maria Isabel Fernandez, Marcos Ortega

PII: S0169-2607(18)30134-2
DOI: 10.1016/j.cmpb.2018.05.033
Reference: COMM 4730

To appear in: *Computer Methods and Programs in Biomedicine*

Received date: 25 January 2018
Revised date: 14 May 2018
Accepted date: 29 May 2018

Please cite this article as: Gabriela Samagaio, AiAda Estévez, Joaquim de Moura, Jorge Novo, Maria Isabel Fernandez, Marcos Ortega, Automatic Macular Edema Identification and Characterization Using OCT Images, *Computer Methods and Programs in Biomedicine* (2018), doi: 10.1016/j.cmpb.2018.05.033

## Highlights

- The automatic detection and extraction of the Macular Edema (ME) regions is a relevant task as it helps significantly in the evaluation of the disease severity.
- A new complete methodology is proposed to analyze and characterize the presence of the ME within the retinal tissue using Optical Coherence Tomography (OCT) images.
- Using the reference clinical classification, the identified intreretinal fluids accumulations types are Serous Retinal Detachment (SRD), Diffuse Retinal Thickening (DRT) and Cystoid Macular Edema (CME).
- The experimental results offer an accurate performance in the identification and characterization of the all the types of ME within the retinal tissue.
- This proposed system represents a useful auxiliary tool, improving the efficiency in the healthcare systems, aiding the clinicians in this complex work of detection and characterization of a relevant disease as is the ME.

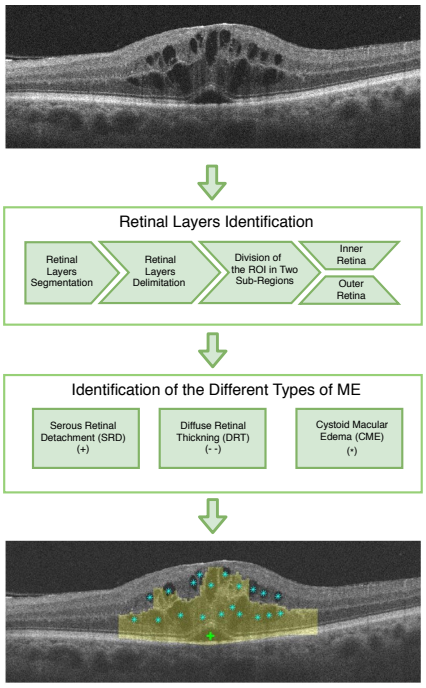

# Automatic Macular Edema Identification and Characterization Using OCT Images

Gabriela Samagaio [a], Aída Estévez [d], Joaquim de Moura [a,b], Jorge Novo [a,b,*], María Isabel Fernandez [c,d,e], Marcos Ortega [a,b]

[a] *Department of Computing, University of A Coruña, A Coruña (Spain)*

[b] *CITIC-Research Center of Information and Communication Technologies, University of A Coruña, A Coruña (Spain)*

[c] *Instituto Oftalmológico Gómez-Ulla, Santiago de Compostela, (Spain)*

[d] *Department of Ophthalmology, Complejo Hospitalario Universitario de Santiago, Santiago de Compostela, (Spain)*

[e] *University of Santiago de Compostela, Santiago de Compostela, (Spain)*



**Abstract**

**Background and objective** The detection and characterization of the intraretinal fluid accumulation constitutes a crucial ophthalmological issue as it provides useful information for the identification and diagnosis of the different types of Macular Edema (ME). These types are clinically defined, according to the clinical guidelines, as: Serous Retinal Detachment (SRD), Diffuse Retinal Thickening (DRT) and Cystoid Macular Edema (CME). Their accurate identification and characterization facilitate the diagnostic process, determining the disease severity and, therefore, allowing the clinicians to achieve more precise analysis and suitable treatments.

**Methods** This paper proposes a new fully automatic system for the identification and characterization of the three types of ME using Optical Coherence Tomography (OCT) images. In the case of SRD and CME edemas, multilevel image thresholding approaches were designed and combined with the application of ad-hoc clinical restrictions. The case of DRT edemas, given their complexity and fuzzy regional appearance, was approached by a learning strategy that exploits intensity, texture and clinical-based information to identify their presence.

**Results** The system provided satisfactory results with F-Measures of 87.54% and 91.99% for the DRT and CME detections, respectively. In the case of SRD edemas, the system correctly detected all the cases that were included in the designed dataset.

**Conclusions** The proposed methodology offered an accurate performance for the individual identification and characterization of the three different types of ME in OCT images. In fact, the method is capable to handle the ME analysis even in cases of significant severity with the simultaneous existence of the three ME types that appear merged inside the retinal layers.

*Key words:* Computer-aided diagnosis; Retinal imaging; Optical Coherence Tomography; Macular edema

---

* Corresponding author. Dep. Computación,Universidade da Coruña, 15071 A Coruña, Spain

*Email addresses:* gabriela.samagaio@udc.es (Gabriela Samagaio), aidaestevez55@gmail.com (Aída Estévez), joaquim.demoura@udc.es (Joaquim de Moura), jnovo@udc.es (Jorge Novo), maribelfernandez@institutogomez-ulla.es (María Isabel Fernandez), mortega@udc.es (Marcos Ortega).

## 1 Introduction

Visual impairment represents a major worldwide health concern which, besides its effects on the normal vision, carries a significant loss of life quality and an important economic cost both to the patients and the healthcare systems. According to the World Health Organization (WHO), it is estimated that 253 million people suffer from visual impairment in the world, where 36 million are blind and 217 million present low vision [1,2]. In the last 10 years, despite the progress that was made in surgical procedures, cataracts still remains as the leading cause of visual impairment affecting a 47.9% of the population with vision difficulties. Macular Edema (ME), especially diabetic ME, is also among the main causes of vision loss, being listed as the second [3]. It is defined as a swell in the macular region caused by the leak of fluid from the retinal blood vessels. This swelling changes the morphology of the retinal tissues, fact that is directly linked to the central vision loss, disabling the individuals to correctly perceive shapes, colors or even details of the objects [4]. In the last decades, the average lifespan has increased, yielding an older population where the vision problems are more frequent. For that reason, it is estimated that the number of people with visual impairment could be triplicated by 2050. It is important that the early detection and treatment of retinal diseases become one of the major health issues in all the countries, especially in the developed ones.

Nowadays, Computer-Aided Diagnosis (CAD) systems are used in ophthalmology as important tools that support the clinical evaluations of several types of eye fundus images. One of the most widely used is the Optical Coherence Tomography (OCT) image modality. This acquisition technique, that

is increasing its popularity and use, provides images of a cross-sectional visualization with high-resolution of the retinal layers. It is a non-invasive and contactless technique that evaluates in vivo the histopathology of the retinal tissue.

Regarding the ME disease, a clinical classification was proposed by Otani *et al.* [5] using OCT images, being widely used worldwide by the specialists as a way to classify the different types of ME based on the properties of the OCT image modality. Hence, considering the clinical characteristics that are present in these images added to retinal properties as thickness, reflectivity or the area of the intraretinal fluid accumulation, MEs were categorized in three main types: Serous Retinal Detachment (SRD), Diffuse Retinal Thickening (DRT) and Cystoid Macular Edema (CME). Posteriorly, Panozzo *et al.* [6] extended this classification with a new proposal that better characterizes these clinical conditions. The new classification takes into account five parameters for the same defined ME types: retinal thickness, diffusion, volume, morphology and presence of vitreous traction [7]. Figure 1 illustrates the complexity and heterogeneity of this retinal pathology, given the significant variability in terms of morphology, shape or the relative position that each ME type normally presents within the retinal tissue. Typically, the SRD type is characterized by a dome shape at the inferior retinal layers whereas the CME type is defined by the presence of the intraretinal cystoid spaces of low reflectivity separated by highly reflective boundaries that represent the intraretinal cystoid-like cavities [8]. Finally, the DRT type is commonly characterized by a "sponge-like" swelling appearance as a result of a regional fluid spread with reduced intraretinal reflectivity [4,9].

An automatic detection and extraction of these ME regions is a crucial task

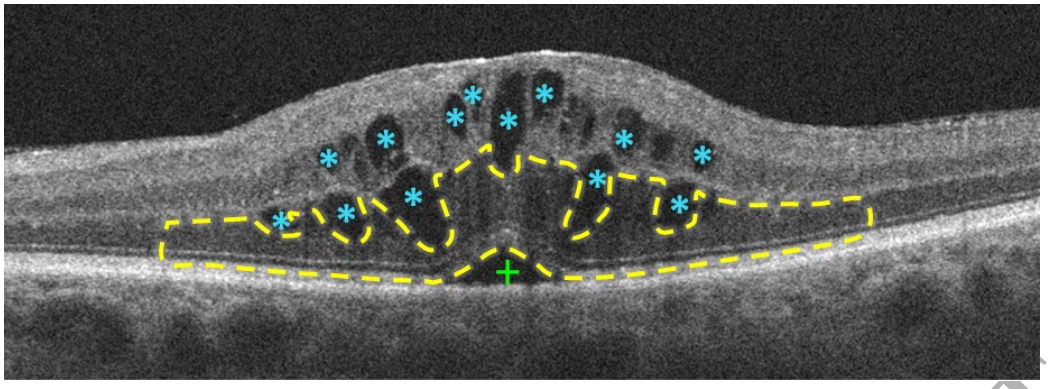

Fig. 1. Example of OCT retinal image with the specified three types of ME: SRD(+), CME(*) and DRT(- -).

as it significantly helps in the evaluation of the disease severity, aiding the clinicians to determine more accurate diagnosis and treatments [10].

In recent years, most of the proposed computational works using OCT images have focused their studies on a general or partial analysis of the presence of the intraretinal fluid. Sidibé *et at.* [11] proposed a technique that allows the classification of the entire OCT volume. This approach is based on modeling the appearance of normal OCT images using Gaussian Mixture Models (GMM), detecting as outliers the images with intraretinal fluids. In the work of Montuoro *et al.* [12], the authors proposed an automatic method based on graph theory that allows the simultaneous segmentation of the retinal layers and the existing fluid-filled regions. Following a similar idea, Alsaih *et al.* [13] used learning strategies to identify normal volumes versus volumes with the ME presence. The dataset was assessed by trained graders and the method identified the volume types in the OCT images based on the evaluation of the retinal thickening, hard-exudates, intraretinal cystoid space formation as well as subretinal fluid. Deep learning was also recently introduced in the issue mainly for cystoid edemas, as the work of Lu *et al.* [14] that proposed a methodology using a Fully Convolutional Neural Network (FCN) for the segmentation of abnormal fluid regions within the retinal tissue. Lee *et al.* [15]

proposed a method for the automatic segmentation of fluid regions by the application of a Convolutional Neural Network (CNN). Using a similar strategy, Gopinath *et al.* [16] proposed a method also using a CNN implementation for the segmentation of CMEs followed by a post-processing step using clustering to refine the previously identified cystoid regions. Roy *et at.* [17] also implemented a convolutional architecture based on the RelayNet to simultaneously segment the retinal layers as well as the fluid regions that are present in the OCT images. Schlegl *et al.* [18] used a neural network comprising two processing components, an encoder that transforms an input image into an abstract representation and a decoder that maps the abstract representation to an output image assigning each pixel to a class as normal or abnormal fluid regions. In the work of Girish *et al.* [19], the authors proposed a FCN to automatically capture both micro and macro-level features for the characterization of the cystoid structures. Rashno *et al.* [20] proposed the application of a neutrosophic transformation and a graph-based shortest path method to segment fluid-associated and cystoid regions. González *et al.* [21] proposed a strategy for the automatic detection of CME edemas. This approach applies a flooding process and a texture analysis, within the retinal region, to identify the presence of these ME type. In the work of Moura *et al.* [22], a method for the automatic identification of intraretinal fluid regions was designed based on a set of features that characterize the analyzed regions, including intensity and texture-based features. Girish *et al.* [23] proposed a benchmark study for the automated intra-retinal CME segmentation. In particular, the authors introduced a modular approach integrating different segmentation algorithms, facilitating the comparative analysis between the obtained quantitative and qualitative results of the experiments. Esmaeili *et al.* [24] proposed a methodology to detect dark pixels between the pigmented epithelium and the nerve

fiber layer considering them as cystoid spaces. This approximation was based on a K-SVD dictionary learning [25] in the curvelet transform [26] to help reducing speckle noise, facilitating the set of thresholds that are posteriorly applied to the regions of interest. Other works as Wu *et al.* [27] focused their study in the detection of SRD edemas. The proposed method involves the construction of a probability map from training samples using a classification process with random forest. This map results from the linear combination of information from image characteristics like the structural texture, intensity or the layer thickness. Sun *et al.* [28] proposed a framework for the SRD edema segmentation that combined AdaBoost classification and a shape-constrained graph cut.

To date, none computational proposed work faced the simultaneous identification of the three ME types, being their presence and corresponding amount relevant information for the characterization of the ME disease, as defined in the clinical guides of reference [5,6]. Additionally, none scientific proposal studied the automatic identification of the specific case of DRT edemas.

The proposed system of the present work aims to achieve a fully automatic and simultaneous detection and characterization of the three types of ME (SRD, DRT and CME) following the indicated clinical classifications of reference in the ophthalmological field. In particular, the system identifies all the appearances of the different ME types within the retinal tissue. This way, all the existing edemas are provided as well as their characterization by type, representing crucial information to determine the degree of severity of the ME disease. Since the retinal fluid accumulation forms swollen regions within the intraretinal tissues, the proposed system firstly delimits and restricts the analysis to the region of the retinal layers. Given that each type of edema typically

appears in particular parts inside these retinal layer tissues, two sub-regions are also identified to facilitate the work: the ILM/OPL (or inner retina) and the OPL/RPE (or outer retina) regions, where the Inner Limiting Membrane (ILM) and the Retinal Pigment Epithelium (RPE) constitutes the limiting membranes of the entire layer retinal area and the Outer Plexiform Layer (OPL) represents the transitional layer. Focusing within these regions, the system combines clinical knowledge, image processing techniques (for the SRD and CME cases) as well as a learning strategy (for the DRT case) to identify the presence of all the existing edemas. Finally, the system presents, as output, a labeled image with all the identified edemas, correctly characterized by type. This way, this process allows the standardization of the identification of the existing ME types, avoiding the subjectivity that is frequently introduced among ophthalmologists in this analysis. Additionally, given the instantaneous performance of an automatic computational procedure, the work of the specialists is facilitated, improving their productivity. This improvement benefits the early diagnosis of the disease and, consequently, the life quality of the patients.

The paper is organized as follows: Section 2 presents the proposed methodology and its main characteristics. Section 3 presents the results and validation of the main stages of the methodology. Section 4 includes the discussion of the obtained results and the challenges that were faced in the work. Finally, Section 5 presents the conclusions about the proposed system as well as possible future lines of work.

## 2 Methodology

The proposed system receives, as input, the histological sections provided by the OCT images. These sections are centered in the macula, as this is the region of analysis where the ME types typically appear, offering an optimal visualization of the retinal tissues to identify the hypothetical presence of ME.

The method aims to the simultaneous identification and localization of the three ME types to characterize their presence or absence as well as their amount, useful clinical information for its visual presentation for posterior clinical analysis. The methodology is composed of a set of progressive stages, as illustrated in the diagram of Figure 2. Firstly, the system detects the 4 main retinal layers in the OCT section that delimits the region of interest (ROI). This retinal area is divided into two sub-regions: inner and outer retina. Posteriorly, the system searches each type of ME in three main steps to identify and characterize them individually.

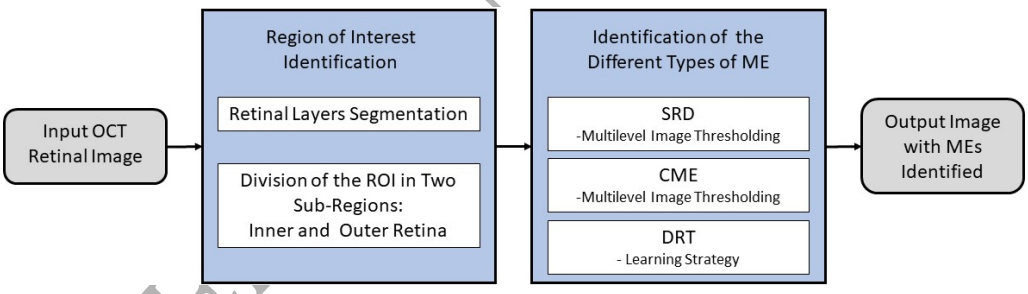


Fig. 2. Main steps of the proposed methodology for the identification of the ME types: SRD, CME and DRT.

For the SRD and CME cases, we used multilevel adaptive image thresholding approaches, whereas for the DRT case a learning strategy was implemented. Posteriorly, as output, the system provides a labeled image with the identifications and associated types for a better characterization and understanding of the present ME disease.

Despite that these three types derive from the same cause, the leak of fluid, their characteristics and visual appearance within the retinal layers are enormously different, due to properties such as morphology, shape, texture or even the relative position within the retinal tissue. These significant differences make the ME disease a particularly complex retinal pathology.

Given their characteristics, two of the cases could be directly approached with image processing strategies (the SRD and CME cases), basing their identification in the initial selection of possible candidates and a posterior removal of wrong detections using the mentioned properties as shape or relative position, among others, to preserve the real existing ones. For the identification of these edemas, all the defined parameters were designed and determined in collaboration with the clinical specialists, as well taken from clinical knowledge of the literature.

The DRT edema generally presents a more complex appearance within the retinal tissue, with a more fuzzy presence and not well-defined boundaries. These characteristics constitute a more complex scenario, motivating the implementation of a learning strategy for their identification, looking for their characteristic texture or clinical properties as the corresponding increment in the retinal thickness, among others, as evidence of their presence.

### *2.1 Identification of the Region of Interest*

The OCT images allow the visualization of the morphology of the retinal tissues. When the pathological structures emerge within the retinal tissue its typical morphology changes significantly. Usually, MEs have specific relative positions within the retinal layers. Therefore, to facilitate the detection of

these edemas, the system firstly identifies the four main retinal layers and, then, sub-divides this ROI in two sub-regions: the inner and the outer retina. This process is described with more detail in next subsections.

### *2.1.1 Retinal Layer Segmentation*

The reconstruction of the OCT images leads to a degradation of the quality of these images, difficulting the differentiation of the subsurface structures [29], as the retinal layers, by the inclusion of speckle noise. For that reason, the speckle noise reduction is a common preprocessing stage in the analysis of OCT images [30]. In that sense, to clean the image and simultaneously preserve the properties of the retinal tissue, a median filter was applied, as a preprocessing, in order to facilitate the posterior identification stages.

Next, four main retinal layers were identified to delimit the search space: ILM, OPL, ISOS and RPE (illustrated in Figure 3). We initially based our proposal in the work of Chiu *et al.* [31]. Using this strategy, our system identifies the ILM, ISOS and RPE layers. This automatic approach mainly uses graph theory and dynamic programming. Hence, an OCT image is represented as a graph of nodes, connecting optimum paths from both sides of the image. Each graph node corresponds to a pixel where the subsequent connected pixels form a pathway from both sides of the image. The optimal paths provide the aimed layers. The algorithm calculates dark-to-light gradient images, identifying adjacent layers and generating weights for the layer segmentations. The main layers of the retina are identified progressively by the minimum weighted paths using the Dijkstra algorithm [32].

As indicated, this approach was used to identify the ILM and RPE retinal

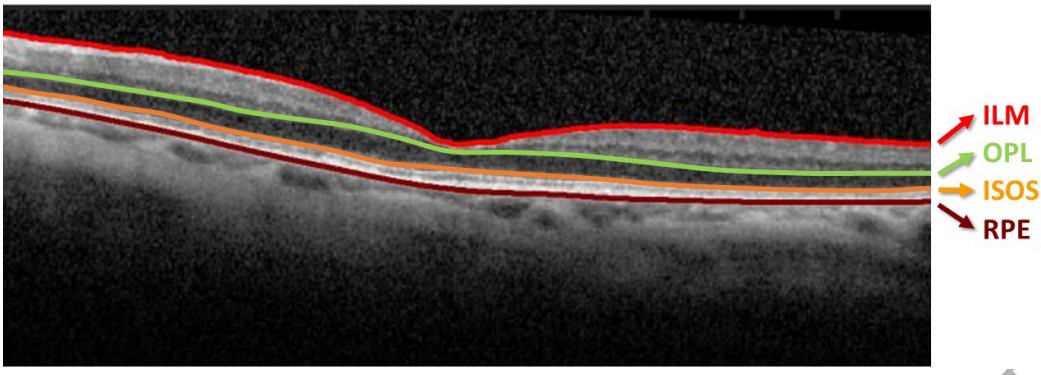


Fig. 3. Example of OCT image with the identification of the aimed four layers: ILM, OPL, ISOS and RPE.

layers, first and last ones, both delimiting the retinal analysis region. Additionally, the ISOS layer is also detected to simplify the posterior identification of the OPL layer.

The presence of MEs implies a significant change in the normal retinal morphology, deteriorating the conditions of the retinal layers and consequently presenting a significant impact in the OPL layer [33]. This layer is significantly altered in its typical morphology by the presence of fluid in the inner and outer retina hardening the identification process. Given that, the previous method did not present acceptable results in very deteriorated pathological cases. For that reason, we implemented a new strategy to identify the OPL layer that offered a robust performance, even in deteriorated cases. To solve this issue, the previous identification of the ISOS layer is used as baseline to extract the region immediately over it that corresponds to the OPL layer. Thus, over the ISOS layer, $N$ initial points are randomly generated and used as seed for region a growing process [34], as shown in Figure 4. The number of generated seeds is proportional to the image dimension, representing an amount of a 10% of the input image width. This strategy progressively appends other pixels with similar properties in the seed points neighborhood. This way, we obtain the entire region over the ISOS layer by intensity similarity. The upper limits

of the resultant region identify the limits of the aimed OPL layer, strategy that is illustrated in Figure 5. The use of a significant number of seeds along the image guarantees the OPL extraction even in deteriorated pathological conditions, as in the presence of ME in advanced stages.

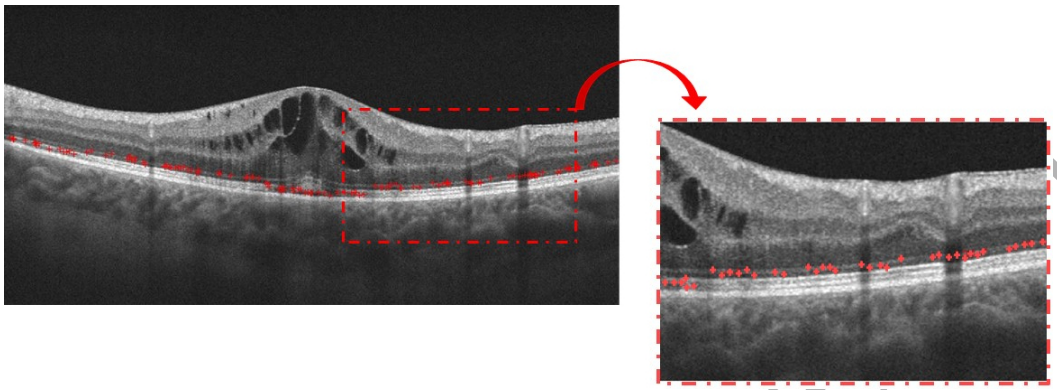

Fig. 4. Example of OCT image with the initialization of N seeds points (+) over the ISOS layer.

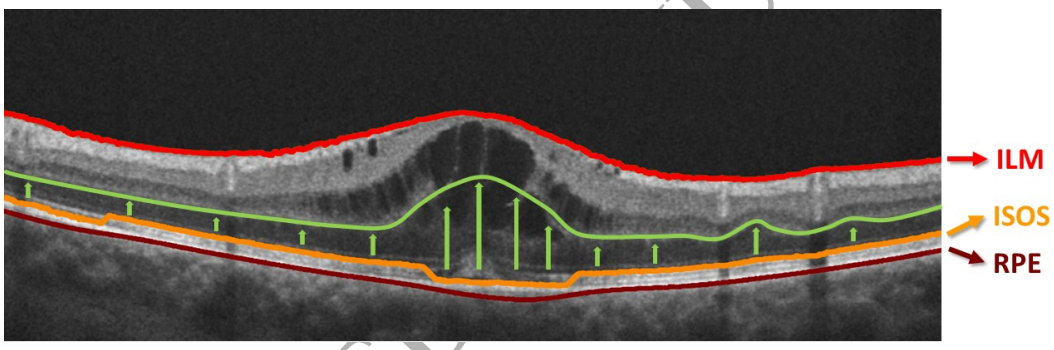


Fig. 5. Example of OCT image with the identification of the OPL layer. The arrows (↑) indicate the direction of growing of the proposed algorithm.

### *2.1.2 Division of the ROI in Two Sub-Regions: Inner and Outer Retina*

In most of the ME cases, edemas are accumulated in typical relative positions within the retina. According to the Otani *et al.* [5] classification, CMEs normally start to manifest symptoms in the inner retinal layers, defined as the upper region of the analyzed ROI. In contrast, SRD and DRT edemas typically appear in the outer retinal layers. In more severe pathological stages, CMEs can proliferate from the inner to the outer retina and merge with DRT

edemas [35]. Based on those premises, two sub-regions are identified inside the ROI as inner and outer retina, using the previously identified retinal layers to facilitate the posterior identification of each type of ME. The inner retina can be defined as the upper region of the ROI, comprehended between the ILM and the OPL layers whereas the outer retina is the lower region, which is limited by the OPL and the RPE layers, as illustrated in Figure 6. As said, the identification of the boundaries of these two regions simplifies the detection of each type of intraretinal fluid accumulation, reducing the search for each ME type.

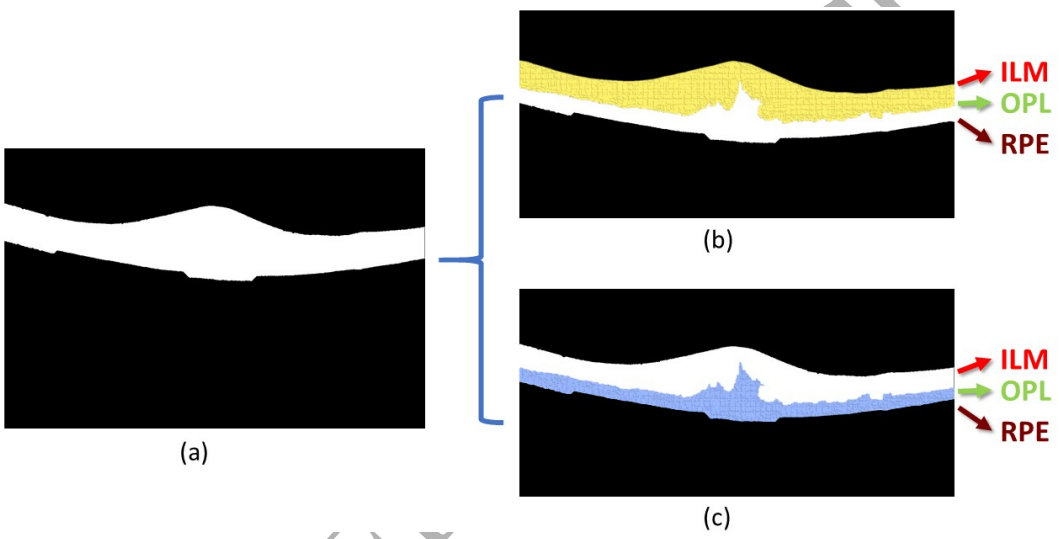


Fig. 6. Inner and Outer retinal regions. (a) The entire ROI, which delimits the retinal tissue between the ILM and RPE layers. (b) The inner retina, between the ILM and the OPL layers. (c) The outer retina, between the OPL and the RPE layers.

### *2.2 Identification of the Different Types of ME*

Each type of ME is searched in the sub-region where they typically appear. Then, image analysis and medical knowledge were combined in individual specific strategies for the detection and localization of each of the three types of ME, given their significant differences in appearance and characteristics.

### *2.2.1 SRD Detection*

SRD edemas appear centered in the macula when the fluid is leaked under the ISOS and over the RPE layer regions, as observed in the example of Figure 7. In the OCT images, it can be recognized by the presence of a hyporeflective space, presenting a characteristic dome-like elevation of a detached retina. These characteristics are mainly used by the specialists for the DRT identification. However, in early stages, it is complicated to distinguish the typical contrast over the photoreceptors layer and the early proliferation of this ME type, difficulting the identification of its presence.

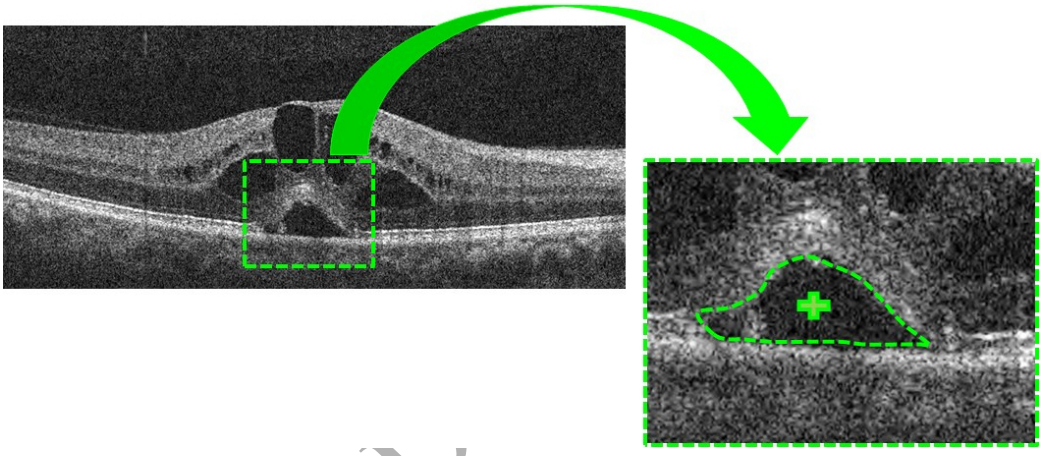

Fig. 7. Example of OCT image with the presence of SRD edema.

The proposed system automatically identifies the presence of SRD edemas using this clinical knowledge as reference. Given the relative position where they typically appear, the proposed strategy was implemented restricting the search space to the previously identified outer retina. Inside this area, an adaptive thresholding [36] was applied in order to segment areas with identical intensity profiles. In this case, the optimal threshold was determined with the value that maximizes the separability between the intraretinal fluid regions and the surrounded retinal layer tissues [37,38]. As a result, different candidates of SRD edemas presenting low intensity profiles are obtained.

Next, we filter clear false positives from the entire set of candidates with a list of medical restrictions that a SRD edema should accomplish:

- *Relative position.* It should be near the ISOS layer and close to the macula [39];
- *Minimum area.* Using as reference the double of the typical area of the Microcystic Macular Edemas (MME), we consider a SRD edema candidate if it presents an area bigger than 200pixels$^2$, equivalent to 4,751$\mu m^2$ [35,40].
- *Morphology.* SRD edemas normally appear with a fusiform shape, also called dome shape. To measure this fusiform shape, we enclose each candidate in an ellipse form. The minor and major axis of the ellipse of the candidate should be respected. It was empirically determined that these parameters should be bigger than 10pixels and less than 250pixels for the minor and major axis, respectively, as the usual dimensions that the SRD edemas typical present in the eye fundus.
- *Constriction of the photoreceptors layer.* The presence of fluid in the macular region leads to a thickness reduction of the region comprehended between the ISOS and the RPE layers [41]. This analysis uses a window that takes, as reference, the column of the centroid of the candidate allowing the determination of the RPE/ISOS thickness in that area. Then, to be considered as possible SRD edema, the local mean thickness should be smaller than 95% of the global ISOS/RPE thickness to consider a notable constriction of the photoreceptors layer.
- *Intensity profile.* These edemas are characterized by a containing hyporeflective region in contrast with the surrounded retinal tissue, which is hyperreflective (produced by the photoreceptors layer). Using the centroid of the candidate, we analyze the intensities of the immediately surrounding tissue using a window with 10pixels of width. Then, to be considered as

a possible candidate the local mean intensity should be bigger than 0.17, value that was empirically determined.

Additionally, this edema is also characterized by its presence near the fovea. Given that a patient can only present a SRD edema, if two or more candidates fulfill these conditions, we only preserve the one closer to the foveal center. Given that the adaptive thresholding process does not produce detailed segmentations, the region of the identified candidate is used as seed for a region growing process to obtain a more adjusted segmentation of the SRD region. This precise extraction is useful for its entire removal in posterior stages of the methodology in the search of the other ME types.

#### *2.2.2 DRT Detection*

DRT edemas are classified by the specialists as a swelling of the retinal thickness, with undefined boundaries and a reduced contrast with the surrounding tissue. The regional leak of fluid within the outer retina produces a pattern typically characterized as a "sponge-like" appearance. However, in some OCT images, these edemas are presented with a bright pattern, whereas in other cases it appears as significantly dark regions, similar to the background of the image. As these edemas occur in the outer retina but above the photoreceptors layer, to search their presence, we remove the photoreceptors region and the SRD edema from the search space, as detected in the previous stage. The previous precise extraction of the SRD edema facilitates its removal from the new region of interest. Additionally, the correction of the OPL/RPE region to the OPL/ISOS region also decreases the detection of false positives with a more precise and restricted region to detect the DRT edema. Given the complexity of this ME type, a learning strategy was applied in this case.

Therefore, each column within the search space is considered using a window of a defined size that is centered in the analyzed column. Since the outer retinal thickness is not constant, the height of the window varies according to the analyzed column, being adjusted to the OPL/ISOS region height. This strategy allows the extraction of features that better describe the DRT edema presence. A suitable ensemble of features based on intensity and texture properties was analyzed in combination with clinical-based information, as the retinal thickness, which is normally increased by the presence of DRT edemas [42].

In detail, the analyzed features, that are summarized in Table 1, are the following:

- *Intensity Image Analysis.* We analyze the global intensity of the region of interest in each column of the OCT image. The "sponge-like" appearance implies the inclusion of a higher irregularity and a drop of the intensity profiles when compared with the normal tissue of the retinal layers. For that reason, we measured 6 global statistics over a window that is centered in the analyzed column to capture these alterations. We calculate: maximum, minimum, mean, median, standard-derivation and variance.
- *Gray-Level Intensity Histogram (GLIH).* Following the same reasoning as before, the intensity alterations also vary the characteristics of the histogram. Obtaining the intensity histogram over the window centered in the analyzed column, the following measurements are calculated: obliquity, kurtosis, energy and entropy.
- *Mask Thickness Analysis.* We analyze the thickness of the regions that are commonly used by the specialists in the clinical analysis of the ME. We consider the thickness of the entire retinal region, the thickness of the outer

Table 1
List of the defined 18 features to identify the DRT presence.

| **Number of Features** | **Feature Specification** |
|---|---|
| 1 - 6 | *- Intensity Image Analysis:*<br>Maximum, Minimum, Mean, Median, Variance and Standard Deviation |
| 7 - 10 | *- Gray-level Intensity Histogram (GLIH):*<br>Obliquity, Kurtosis, Energy and Entropy |
| 11 - 14 | *- Mask Thickness Analysis:*<br>Thickness of OPL/RPE region,<br>Thickness of ILM/RPE region and<br>The maximum height of the OPL/RPE region<br>The ratio between the thickness of OPL/RPE and the ILM/RPE regions |
| 15 - 18 | *- Texture Analysis:*<br>GLCM texture-based features: Contrast, Energy Correlation and Homogeneity |

retina (OPL/RPE region) and the ratio between them. This is based on the concept that the presence of intraretinal fluids leads to an increase of the retinal thickness, especially in the outer retina. Therefore, the evaluation of the thickness of these retinal regions is an important medical parameter for the determination of the DRT presence.

- *Texture Analysis.* The "sponge-like" appearance represents a typical texture that these edemas normally present. For that reason, we capture the patterns of the normal retinal tissue as well as the irregularities of the DRT presence using the Gray Level Co-occurrence Matrix (GLCM) texture-based features [43] in order to capture these texture patterns. From the GLCM descriptors we obtained: contrast, correlation, energy, and homogeneity.

The previously defined set of 18 features was posteriorly analyzed using three

different feature selectors: Sequential Forward Selection (SFS) [44], Robust Feature Selection (RFS) [45] and SVM-Forward Selector (SVM-FS) [46]. These feature selectors were successfully applied in similar medical imaging studies [47], to simultaneously reduce the array dimensionality using different strategies but preserving those features with the highest discriminative power. In particular, SFS adds each feature to the subset by an incremental importance order, whereas RFS identifies the features using an emphasizing joint $\ell_{2,1}$-norm regularization selecting those with joint sparsity. SVM-FS uses a linear $\ell_1$-norm SVM for the variable selection, but a non-linear $\ell_1$-norm SVM is used for predicting the best subset.

Using the selected features, two representative classifiers were used to test the potential of the implemented approach: the Naive Bayes and the SVM classifiers. The Naive Bayes classifier [48] is based on the so-called Bayesian theorem whereas the SVM classifier [49] builds a model as a non-probabilistic binary linear classifier.

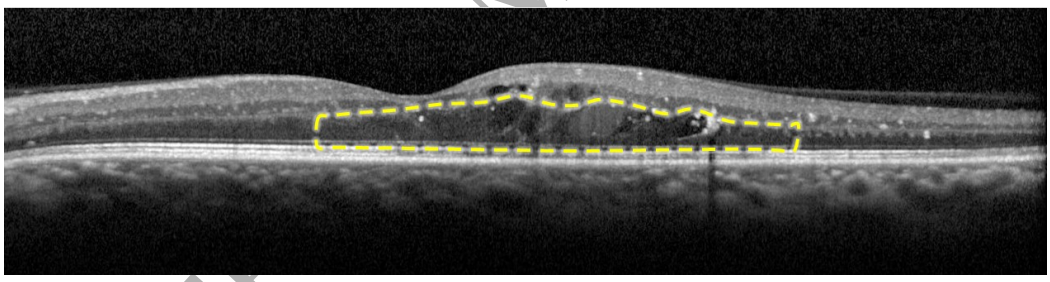

Fig. 8. Example of OCT image with the presence of DRT edema (- -).

Finally, a post-processing stage was implemented to rectify misclassifications originated by other structures that may be present in the eye fundus, such as hard-exudates or vessels, as illustrated in Figure 9. These structures produce shadows on the posterior layers creating dark patterns with different properties in the retinal tissue that can be confused with non-DRT candidate columns [50]. To improve the results, we used an aggregation factor ($d$), to join discon-

nected groups of DRT identifications. This parameter allows the unification of two consecutive DRT regions, when the distance between both detections is smaller than the defined $d$ factor. In those cases, we assume that both detections belong to the same DRT edema, correcting the intermediate non-DRT classified columns. This way, we obtain grouped DRT regions that are more adjusted to the real scenario, improving the performance of the system.

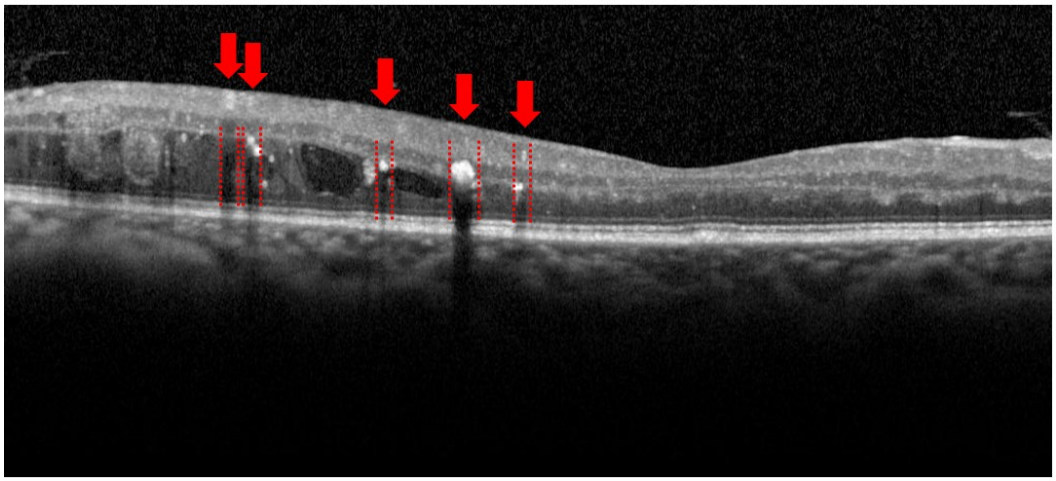

Fig. 9. Example of OCT image with the presence of pathological structures (hard-exudates) and vessels, whose columns are delimited by (- -).

### *2.3 CME Detection*

CMEs are spaces within the retinal tissue typically characterized as cystoid areas with a low intensity profile, as illustrated in the example of Figure 10. Their morphological shape could vary from a well-defined round shape to a petaloid-like appearance (like petals of flowers). They typically emerge in the inner retina with a significant contrast with the surrounded tissue, and a considerable variability in terms of size. In more severe cases, the size of these edemas can be significantly increased, thus, expanding the thickness of the retina, even eventually emerging in the outer retina.

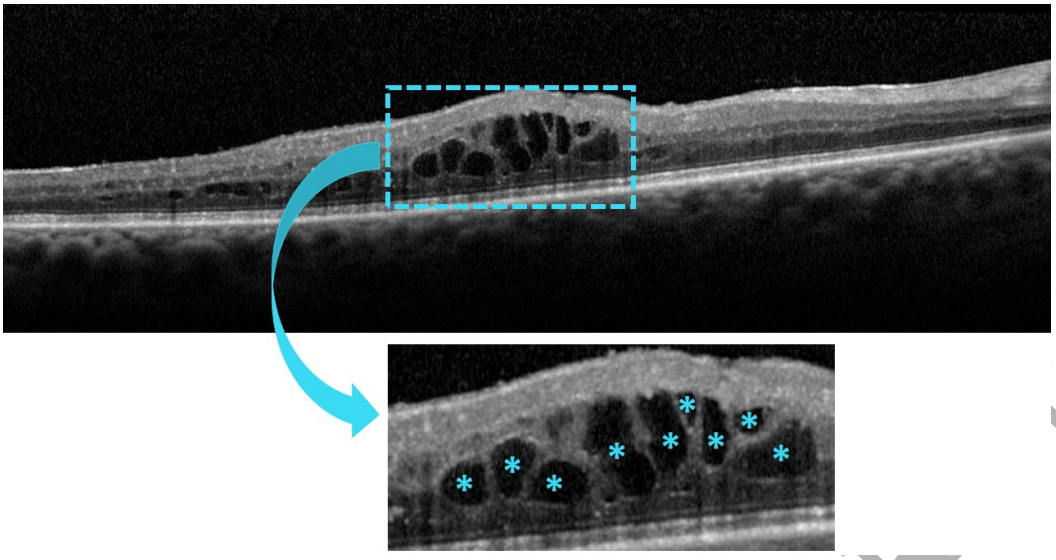

Fig. 10. Example of OCT image with the presence of CME (*).

The proposed system firstly searches the presence of these edemas in the inner retina and then in the outer retina. This strategy was adopted given that the contrast and the characteristics of CMEs in both regions are slightly different. In the inner retina, CMEs typically present well defined boundaries with a clear contrast with the surrounding neighborhood whereas in the outer retina they present a poor contrast between these edemas and the surrounding tissue, hardening their detection and representing a more challenging task. This is illustrated in Figure 11, where an advanced pathological case includes the presence of CMEs in the outer retina, where the poor contrast they normally present in this specific region of the eye fundus is clearly observed.

Considering the typical elliptical shape and the low intensity profiles that this edema presents in contrast of the surrounding tissue of both retinal regions, we implemented adaptive thresholding approaches to identify all the CME candidates. This strategy presents, as main limitation, the possibility of production of partial segmentations of the same candidate cyst. For that reason, in a post-processing stage, we applied a segmentation method based on a flooding process of the image gradient to merge and obtain more defined and reliable

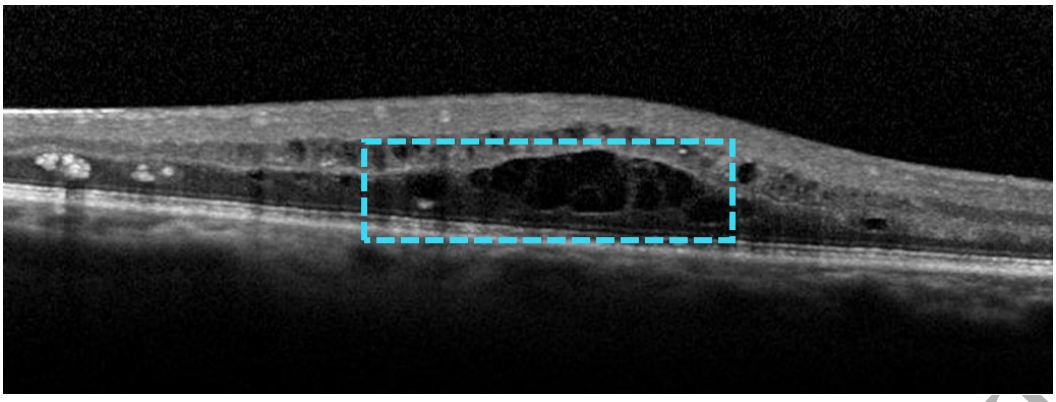

Fig. 11. Example of OCT image with the presence of CMEs in the outer retina (- -). The contrast between the intraretinal fluid and the OPL/RPE region is low, in opposition to CMEs in the inner retina.

extracted regions of the candidates [51]. Posteriorly, we analyzed the entire set of CME candidates to filter any existing false positive using a set of conditions derived from clinical references in the field [4,40,52] and medical knowledge from the specialists that participated in the work. The applied conditions in both regions are:

- *Area size*. This strategy is applied to discard candidates produced by noisy and tissue artifacts such as shadows, among others, that affect both retinal regions. Therefore, the empirically determined minimum areas in the inner and outer retinas were set to $118\mu m^2$ (equivalent to $5\text{pixels}^2$) and $237\mu m^2$ (equivalent to $10\text{pixels}^2$), respectively.
- *Major and minor axis of the surrounding ellipse*. Having the candidate surrounded by an enclosing ellipse, the corresponding minor and major axis of this ellipse are included in the analysis. As limiting conditions, the minor and major axis lengths should be bigger than 7pixels and smaller than 200pixels, respectively. These values were empirically determined as the minimum values that CMEs usually present.
- *Retinal Thickness*. The entire retinal region should have a retinal thickness bigger than $250\mu m$. This value represents the normal thickness of the retinal

tissue of the parafoveal region. When CMEs are present within this region the retinal thickness is significantly increased [4,42].

- *Eccentricity.* To measure this parameter, we take advantage of the axis of the previously defined enclosing ellipse. In particular, the eccentricity is the ratio of the distance between the central point of the ellipse and its major axis length. As CMEs normally present an ovoid shape, we demanded a minimum eccentricity of the candidate, that should be smaller than 0.98.

## 3 Results

The proposed system was validated using OCT images that were captured with a SD-OCT imaging with OCT - Spectralis® OCT confocal scanning laser ophthalmoscope from Heidelberg Engineering. The OCT scans were obtained using a configuration of 7 Line Rater scan with a 30°× 5°of angle of capture and with a space of 240$\mu$m apart from each other. In this study, we used a total of 170 OCT images centered in the macula, with a resolution of 2,032 × 596 pixels. The images correspond to scans from both left and right eyes of different individuals presenting a varying degree of the ME disease, in many cases with many appearances of the three ME types in a single scan. The local ethics committee approved the study and the tenets of the Declaration of Helsinki were followed. To ensure the anonymity of the patients that participate in this study, the corresponding images were renamed by the ophthalmologists before being provided for the system validation.

The system is composed by two main stages: region of interest delimitation and identification of all the appearances of the different ME types. Firstly, the proposed system identifies two regions: the inner and the outer retina.

Given the alternative proposal for the OPL layer extraction, to measure the efficiency of this designed stage, an expert clinician labeled 20 representative OCT images, 10 pathological and 10 non-pathological images, both from the present dataset. For this analysis, two retinal layers were labeled by a specialist: the OPL and the RPE layers. These segmented layers are used to quantify the OPL layer extraction and, consequently, the outer retina identification. A total of 47,136 marked points were obtained from both retinal layers. To measure the performance of this proposal, three statistical, used in similar validation processes [53], were implemented: Mean Absolute Difference (MAD), Correlation Coefficient (CC) and Dice Coefficient (DC) (Equations 1, 2 and 3, respectively). The MAD metric analyzes the absolute mean difference, in pixels, between both segmentations of the OPL layer (manual and proposed method). The CC metric determines the correlation between them. Finally, the DC metric compares the similarity between both segmentations of the entire outer retina, which is delimited by the OPL and the RPE layers as superior and inferior boundaries, respectively.

$$MAD = \frac{1}{N}\sum_{k=1}^{N} m_i - p_i \tag{1}$$

$$CC = \frac{\sum_{k=1}^{N} m_i p_i}{\sqrt{\sum_{k=1}^{N} m_i^2 \sum_{k=1}^{N} p_i^2}} \tag{2}$$

$$DC = \frac{2\sum_{k=1}^{N} |m_i \cap p_i|}{\sum_{k=1}^{N} |m_i| + \sum_{k=1}^{N} |p_i|} \tag{3}$$

where $m_i$ and $p_i$ represent the manual detection and the output of the proposed method, respectively, at the i$^{th}$ (i=1...N) column in two measurements of the OCT image dimensions.

Table 2 presents the results obtained by the proposed system for the OPL

layer and the outer retina identifications. In particular, as global performance, in non-pathological and pathological cases our proposal achieved values of 1.51 pixels for MAD, 99.97% of CC and 0.9439 of DC metrics, representing satisfactory results.

Table 2
Performance of the proposed method for the OPL layer and outer retina identifications in non-pathological and pathological OCT images.

| **Cases** | **MAD (pixels)** | **CC** | **DC** |
|---|---|---|---|
| **Non-pathological** | 1.951 | 99.96% | 0.9623 |
| **Pathological** | 1.077 | 99.98% | 0.9255 |
| **Global** | 1.514 | 99.97% | 0.9439 |

Regarding the edema identification process, in each of the extracted regions, inner and outer retina, the system identifies all the existing edemas of the three ME types in terms of locations and amount. Given that, to validate the proposed methodology, an expert clinician labeled the images indicating the regions with the presence of the three types of ME. Regarding the SRD and CME extraction approaches, we directly compared the identification of the system and the manual identifications of the specialist. In the DRT case, we use the expert labeling by columns, as reference, to construct the training and test sets of the implemented learning strategy. This stage was validated using the following metrics: Precision, Recall, Accuracy and F-Measure. Mathematically, these metrics are formulated as indicated in Equations 4, 5, 6 and 7, respectively. F-Measure is defined as a combination of both precision and recall metrics in a global measurement of the performance of the system.

$$Precision = \frac{TP}{TP + FP} \tag{4}$$

$$Recall = \frac{TP}{TP + FN} \tag{5}$$

$$Accuracy = \frac{TP + TN}{TP + TN + FP + FN} \tag{6}$$

$$F - Measure = 2 * \frac{Precision * Recall}{Precision + Recall} \tag{7}$$

Regarding SRD and CME edemas, as gold standard, formally, we consider the following cases:

- True Positive (TP): we verified if the central point of each detected edema matches with any identification of the specialist. In the case of two or more candidates match with the same manual identification, we only consider the first candidate to ensure the method efficiency.
- False Positive (FP): if the central point does not overlap with any manual identification of the specialist.
- False Negative (FN): if any manual labeling of the specialist is not covered with any central point provided by the system.
- True Negative (TN): otherwise. Given the significative unbalance between both positive and negative sets, TNs are not considered with these edema types.

In the case of the DRT edemas, the same analysis is performed by columns, where we used, as gold standard:

- True Positive (TP): if a column indicated by the ophthalmologist with DRT presence was classified as DRT by the proposed system.
- False Positive (FP): if a column indicated by the ophthalmologist with non-DRT presence was classified as DRT by the proposed system.
- False Negative (FN): if a column indicated by the ophthalmologist with DRT presence was classified as non-DRT by the proposed system.
- True Negative (TN): if a column indicated by the ophthalmologist without

DRT presence was classified as non-DRT by the proposed system.

SRD edemas are a particular and less frequent case as it only affects a reduced group of patients [5]. Moreover, if present, we can only find one per scan. For that reason, the used dataset of 170 OCT images only contains 10 SRD edemas. We would like to remark that the 10 cases were correctly identified by the proposed system.

Regarding the DRT detection, a learning strategy was applied using both Naive Bayes and SVM classifiers. For that, we used a window size with a width of 5 columns empirically determined, and a variable height summing a total of 5,600 samples extracted from DRT and non-DRT regions to train and test the classifiers without any preprocessing or application of correction parameters. This dataset was divided into two subsets, one for training and the other for testing. Next, to ensure the global performance of the method, we trained both classifiers using a 10-fold cross-validation using 10 repetitions, being calculated the mean error/accuracy to determine the most suitable configuration for each case using the best performances. Then, using the best configuration of each classifier, we proceed with the corresponding validation processes using the testing data. We tested the performance of the system with 51,346 columns containing DRT and 68,976 non-DRT edemas.

To detect the DRT edemas, firstly, three feature selectors (RFS, SVM-FS and SFS) were applied to determine the subset of features that better discriminate the presence of this ME type. The majority of the selected features were taken from intensity image analysis, mask thickness and GLCM texture-based features, as they present the highest capacity of differentiation between DRT and non-DRT patterns.

Table 3 lists the performances in the test set for each classifier and the optimal subsets of each analyzed feature selector. The best configuration for the Naive Bayes classifier obtained an accuracy of 87.49% using the RFS subset, whereas for the SVM classifier obtained an accuracy of 86.14% using the SFS subset.

Table 3
Obtained results by the analyzed classifiers and the selected feature subsets.

| **Classifier** | **Selector** | **F-Measure** | **Accuracy** |
|---|---|---|---|
| Naive Bayes | RFS | **84.45%** | **87.49%** |
| | SVM-FS | 84.39% | 87.44% |
| | SFS | 84.36% | 87.41% |
| SVM | RFS | 82.72% | 86.10% |
| | SVM-FS | 82.75% | 86.12% |
| | SFS | **82.79%** | **86.14%** |

Complementary, Table 4 details the performances achieved with both classifiers using a window width of 5 columns. As it can be observed, both classifiers showed a satisfactory behavior in the detection of DRT edemas, being the Naive Bayes classifier slightly better, reaching a F-Measure of 84.45%.

Table 4
Obtained results for the DRT detection using the best configurations of Naive Bayes and SVM classifiers using the testing dataset.

| **Classifier** | **Precision** | **Recall** | **F-Measure** |
|---|---|---|---|
| **Naive Bayes** | 89.88% | 79.65% | 84.45% |
| **SVM** | 88.09% | 78.08% | 82.79% |

Then, we also tested the use of the aggregation factor, $d$, to merge isolated candidates of the same DRT regions. Figure 12 shows the obtained F-Measures in the calculation of the optimal aggregation factor using both classifiers. A more detailed information is listed in Table 5, where the best aggregation factor for the Naive Bayes classifier is $d$=72, whereas for the SVM classifier is $d$=21, reaching a F-Measure of 87.54% and 85.22%, respectively.

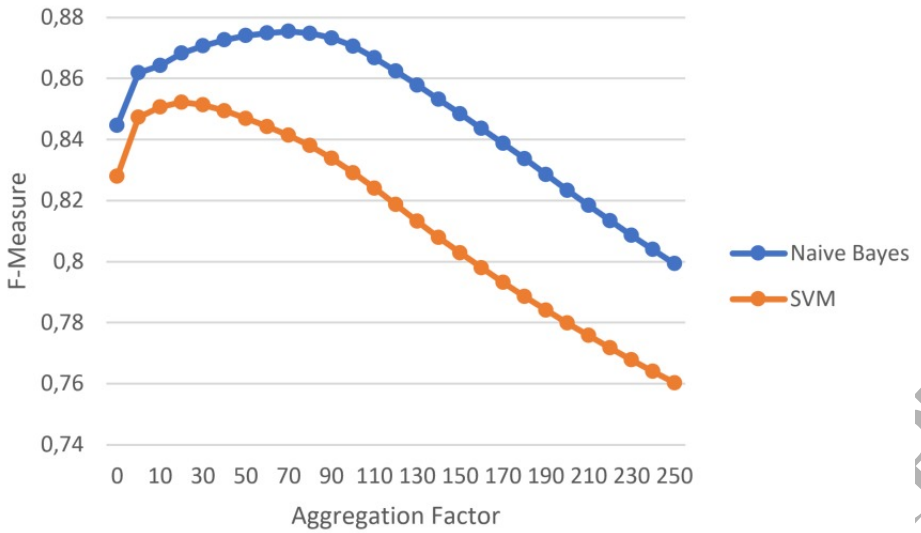


Fig. 12. Determination of the optimal aggregation factor. Obtained F-Measures.

Table 5
F-Measures that were obtained with the tested classifiers and their corresponding optimal aggregation factors using the testing dataset.

| **Classifier** | **Aggregation Factor** | **Precision** | **Recall** | **F-Measure** |
|---|---|---|---|---|
| **Naive Bayes** | $d$=72 | 85.65% | 89.51% | 87.54% |
| **SVM** | $d$=21 | 81.94% | 88.78% | 85.22% |

Figure 13 illustrates an output of the proposal of the best aggregation factor that unifies single candidates in grouped "sponge-like" edema detections.

In the case of CMEs, we divided the evaluation process in the detection in both inner and outer retina. We tested the performance of the system with 379 CMEs that were identified by the specialist in the entire image dataset. The obtained results are summarized in Table 6, where F-Measure reached values of 96.08% and 81.65% in the inner and outer retina, respectively. Finally, as global performance, the system obtained an accurate F-Measure of 91.99%, as also illustrated in Figure 14.

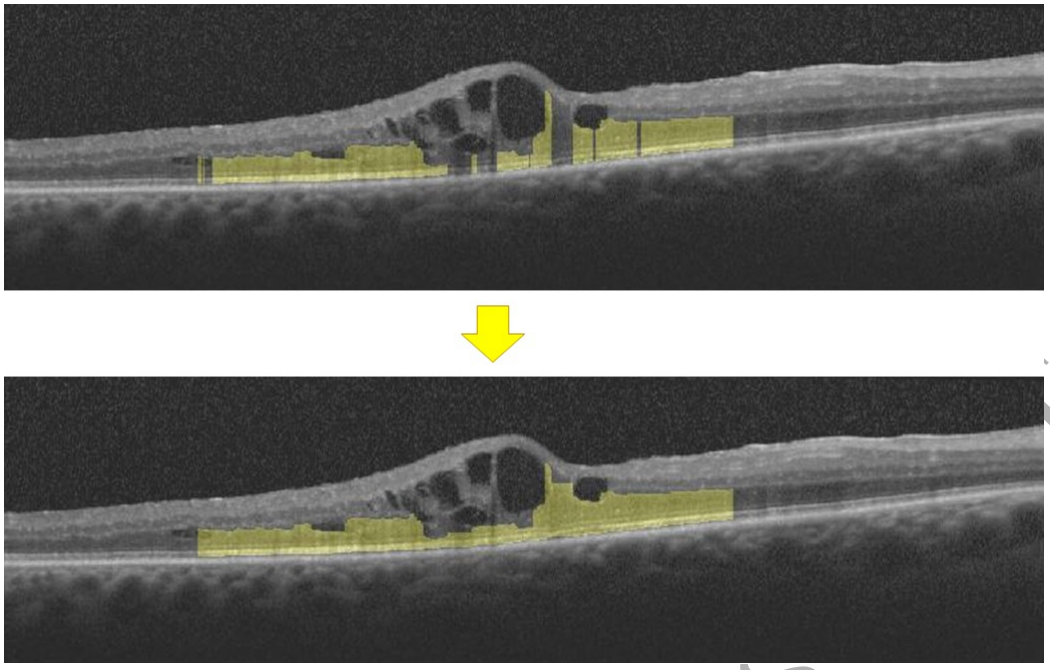

Fig. 13. OCT image with DRT presence. The application of the aggregation factor unifies single candidates in a grouped "sponge-like" edema detection.

Table 6
Results of the CME detection using Precision, Recall and F-Measure.

| Region | Precision | Recall | F-Measure |
|---|---|---|---|
| **Inner Retina (ILM/OPL)** | 97.03% | 95.15% | 96.08% |
| **Outer Retina (OPL/RPE)** | 74.17% | 90.82% | 81.65% |
| **ROI (Inner and Outer Retina)** | 90.13% | 93.93% | 91.99% |

## 4 Discussion

OCT images have become an important auxiliary tool in clinical routines and scientific studies, helping the clinicians in the diagnosis and evaluation of the severity of many diseases.

Given that, we propose a system that firstly segments the inner and the outer retina. In each of these identified regions, three fully automatic strategies were implemented to individually identify the three types of the ME disease.

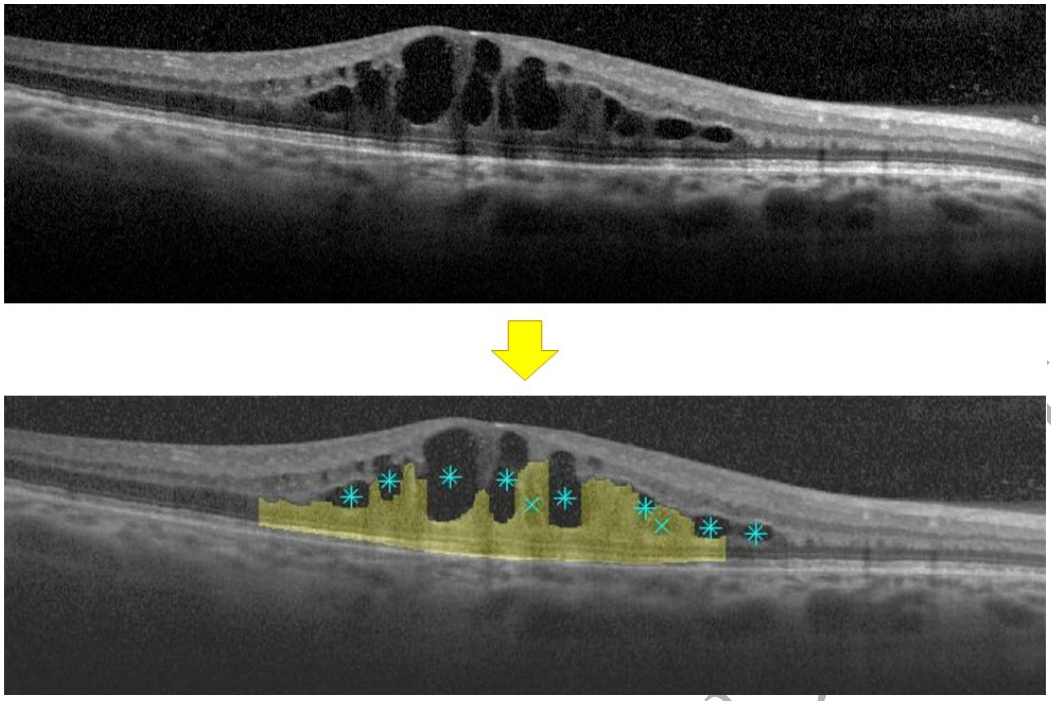

Fig. 14. Example of OCT image with the detection of CMEs (*) in both retinal regions. In particular the CMEs (x) in the outer retina are surrounded by the presence of a DRT edema.

Generally, this issue presents as a main limitation the complex characteristics typical of the OCT images such as the lack of tissue details, the speckle noise or the poor soft tissue contrast in some acquisition scenarios.

Regarding the identification of the upper limiting membrane of the outer retina, the OPL layer, we quantitatively compared the results of our approach with the performance of the work proposed by Chiu *et al.* [31]. The decision of using this alternative approach was motivated by the poor results in the extraction of the OPL layer by the original method in advanced pathological images that, in our case, represent the most frequent scenario. Given that, we compared the performance of both methods in non-pathological and pathological OCT images. As illustrated in Figure 15, both methods present a similar performance for the identification of the OPL layer and the outer retina in non-pathological OCT images (Figure 15 (a), (c) & (e)), whereas in patho-

logical OCT images, the performance of the proposed system is significantly better in comparison with the original method.

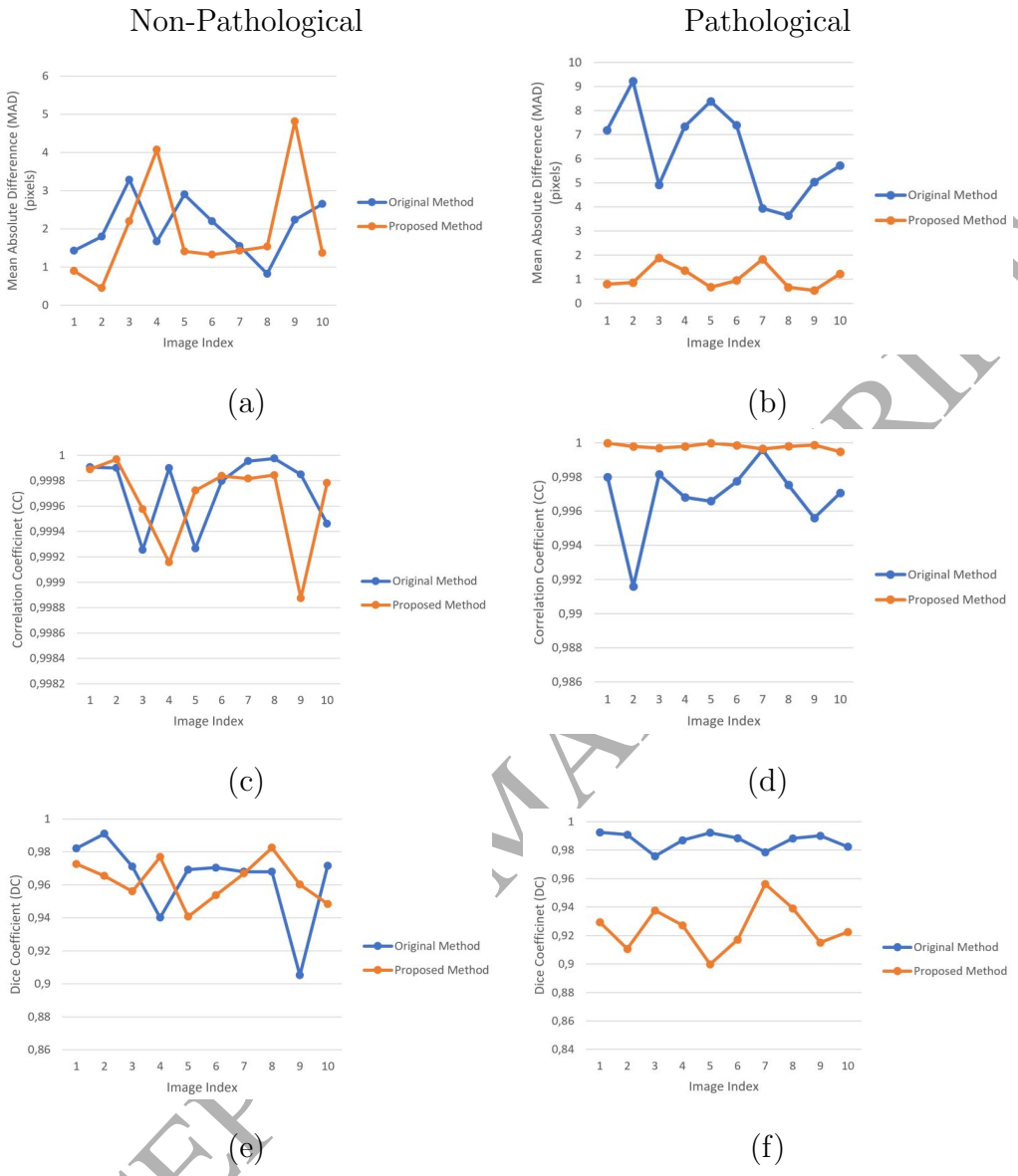


Fig. 15. Comparative analysis between the performance of the original method and our proposal for the OPL layer and the outer retina identifications, using non-pathological ($1^{st}column$) and pathological cases ($2^{nd}column$). (a) & (b) Using MAD metric over the OPL extraction. (c) & (d) Using CC metric over the OPL extraction. (e) & (f) Using DC metric over the entire outer retina segmentation.

Figure 16 illustrates these situations with examples of both non-pathological and pathological OCT images. As we can see, in accordance with the metrics, both methods present a favorable performance for the OPL layer extraction in

non-pathological OCT images (Figure 16 (a) & (b)). However, in pathological images, the original method provides poor results of the OPL layer, crossing the entire macular region (Figure 16 (c) & (e)). In opposition, our proposal detects efficiently this layer (Figure 16 (d) & (f)), facilitating the posterior division of the retinal layers in the consequent inner and outer retina.

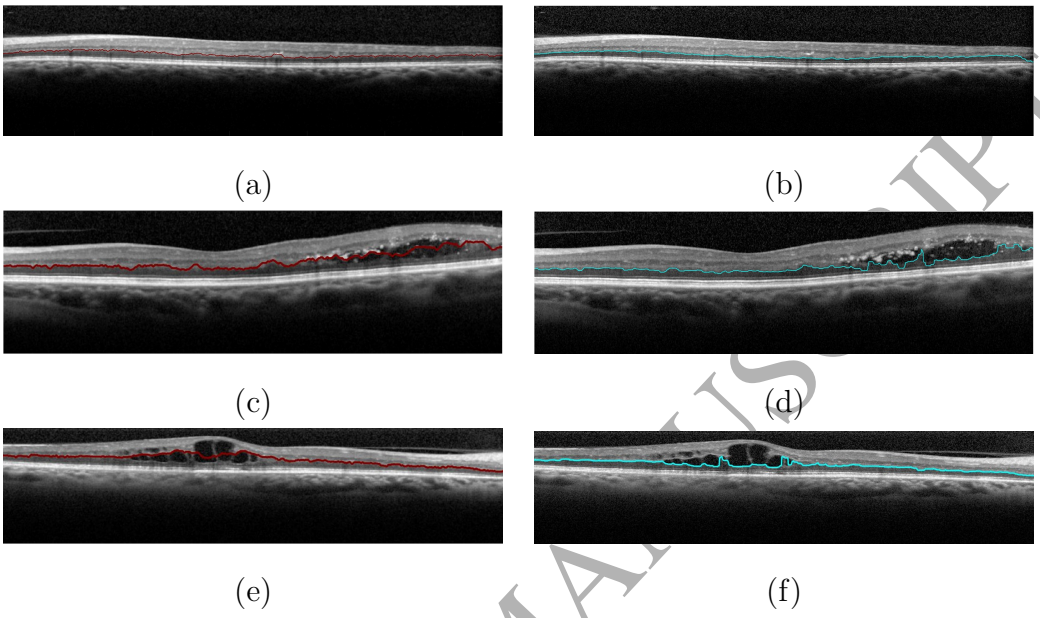


Fig. 16. Example of OCT images with the OPL identification from the output of the original method and our proposal. $1^{st}row$, non-pathological OCT images. $2^{nd}$ & $3^{rd}rows$, pathological OCT images.

Despite the high variability and complexity of the ME disease, the proposed system using the implemented specific strategies is capable of detecting efficiently the hypothetical presence of the three types of ME, even when they appear simultaneously in the same OCT image. Each of these strategies work independently with respect to the others, identifying each faced ME type. The output binary identifications of the three strategies are finally combined to provide the final image result to the specialists to ease their inspection, as illustrated in Figure 17.

SRD edemas constitutes an unfrequent particular case. In this case, the typical contrast of the photoreceptors layer is similar to the presence of this ME type

in early stages, which difficult its identification in some cases. Even in such cases, the system correctly performed the SRD identifications. Similar works present in the literature also detect all the SRD cases [18,27,28]. However, this comparison presents some limitations, given that each study was made using their own image dataset.

In the case of the DRT edemas, to date, no scientific proposal studied the issue of the automatic detection and identification of this ME type. This challenge is related with the absence of limiting membranes as well as the significant pattern variability, difficulting the correct identification of the retinal regions affected by this ME type. Given that, a learning strategy was applied to detect the presence of this edema in the outer retina. In the validation performance, three feature selectors were used: RFS, SVM-FS and SFS. Also, two classifiers were analyzed: Naive Bayes and SVM. Regarding the selected features, the majority of them were taken from the intensity image analysis, mask thickness and GLCM texture-based features. These features are in concordance with the characteristics of the DRT edemas, once they are characterized with "sponge-like" patterns with a significant variability in terms of intensities. Given that, features such as maximum, mean, variance and standard deviation from the global intensity features and the correlation from the GLCM features were mostly selected. Additionally, the thickness of the ILM/RPE and the ratio between the OPL/RPE and ILM/RPE layers were also selected in the first positions as the DRT presence typically implies not only an increment of the outer retina thickness but also the increment of the entire "retinal thickening".

Using the previously selected features, both classifiers were trained and tested using the best configuration. Comparing the results of Table 4 and Table 5, we can conclude that the application of the aggregation factor increases sig-

nificantly the accuracy in the case of the Naive Bayes classifier, as illustrated in the example of Figure 13. In the case of the SVM classifier, this increment was lower. Generally, this difference is given by the SVM, which is more sensitive to noise. For that reason, it produces sets of candidate columns of a variable size in both non-DRT and DRT regions. Instead of that, Naive Bayes presents a considerable number of consecutive candidate columns in the DRT region with a small distance between them. In this situation, the use of the aggregation factor is crucial, merging this small separated DRT detections in coherent merged ones and being this case the one that obtained a higher improvement of this step of the method. This factor benefits the Naive Bayes classifier by connecting significantly close DRT detections whereas this penalizes the SVM case by merging non-DRT with DRT regions. With large values, the aggregation factor groups regions that are too far from each other, decreasing progressively the obtained results.

Regarding the CME detections, we defined two main steps to detect the presence of CMEs in the inner and outer retina, individually. Hence, the system firstly detects these edemas in the inner retina (ILM/OPL), where they present a higher contrast and well-defined boundaries, allowing a better identification of the fluid regions. For that reason, the performance of the system in this first region is significantly better. Despite the large variability in terms of size and shape, the implemented approach successfully identified the CMEs, as shown in Figure 17. In fact, the proposed system was capable to detect even cystoid edemas with complex petaloid shapes that appear often merged even between both regions.

Most of the missed CMEs present specific and uncommon morphologies and

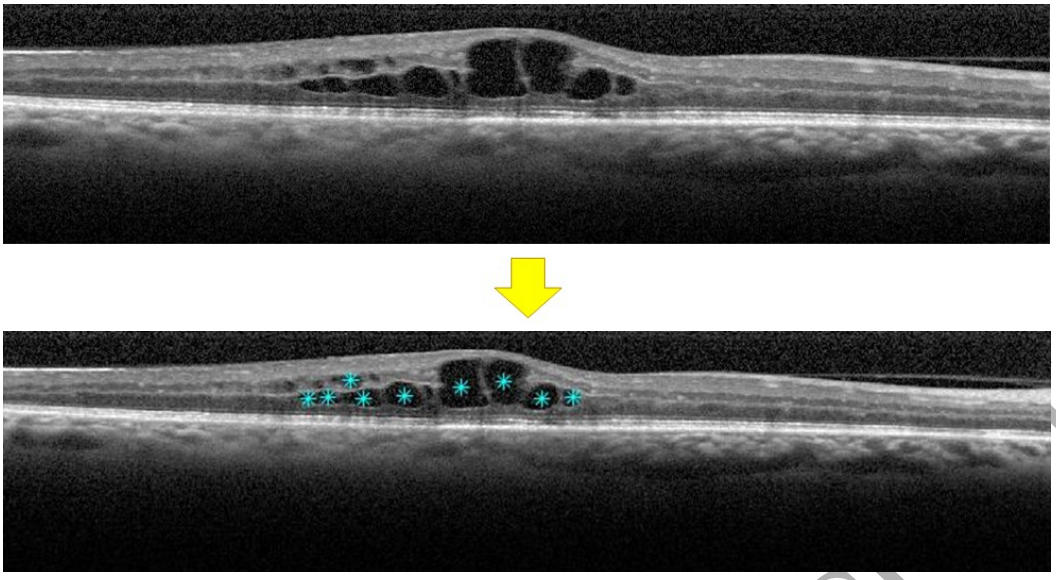

Fig. 17. Example of OCT image with the presence of CMEs (*).

sizes, such as those with fusiform shapes or cystoid edemas with reduced areas. Figure 18 presents an illustrative example of the first case with the presence of a cyst with an unusual horizontal elliptical shape.

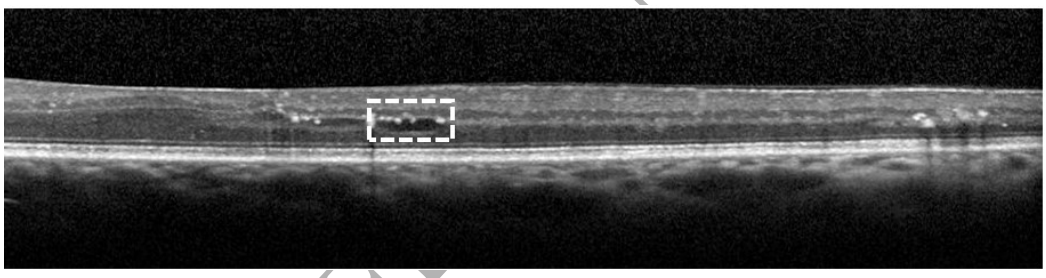

Fig. 18. Example of OCT image with a non-detected CME (- -), with an elliptical horizontal shape.

In the case of small edemas, they are easily mistaken with noise and other artifacts that are typically present in the OCT images. In fact, as explained, the system removes small identifications considering the sizes that noisy and artifact detections typically present in the inner and outer retina. This restriction also avoids the detection of any present microcyst, being out of the scope of this work.

Moreover, the presence of fuzzy contours further complicates the detection

of these edemas. Additionally, when these edemas are proliferated in nearby groups, their individual identification is more complex to accomplish.

Then, the performance of the system was tested in the outer retina. As indicated, in this region, CMEs do not present well-defined boundaries, being frequently mistaken with the surrounded tissues given the almost absent contrast between these fluid accumulations and the neighboring retinal tissues. Moreover, many times, in advanced pathological cases, CMEs are surrounded by the presence of DRT edemas, hardening the identification of the CME locations. Consequently, the accuracy of the method is decreased in this region but still with a satisfactory performance (Table 6).

We proposed a system for the individual identification of the three types of ME that is also capable of their identification when they appear simultaneously in the OCT scans. This is illustrated in Figure 20 with examples of the individual and the merged presence of the different ME types. Firstly, we can see satisfactory individual identifications of SRD edemas (Figure 20 (a) & (b)), DRT edemas (Figure 20 (c) & (d)) and CME edemas (Figure 20 (e) & (f)). We also present the simultaneous detection of DRT and CME cases (Figure 20 (g) & (h)) where we can see that the proposed system is capable to identify them even if they appear merged. This idea is also presented in the representative case of Figure 19 with a scan with ME presence in an advanced stage. In this case, we can see the accurate performance of the system with the simultaneous detection of the three types that are present in the retinal layers in this single scan.

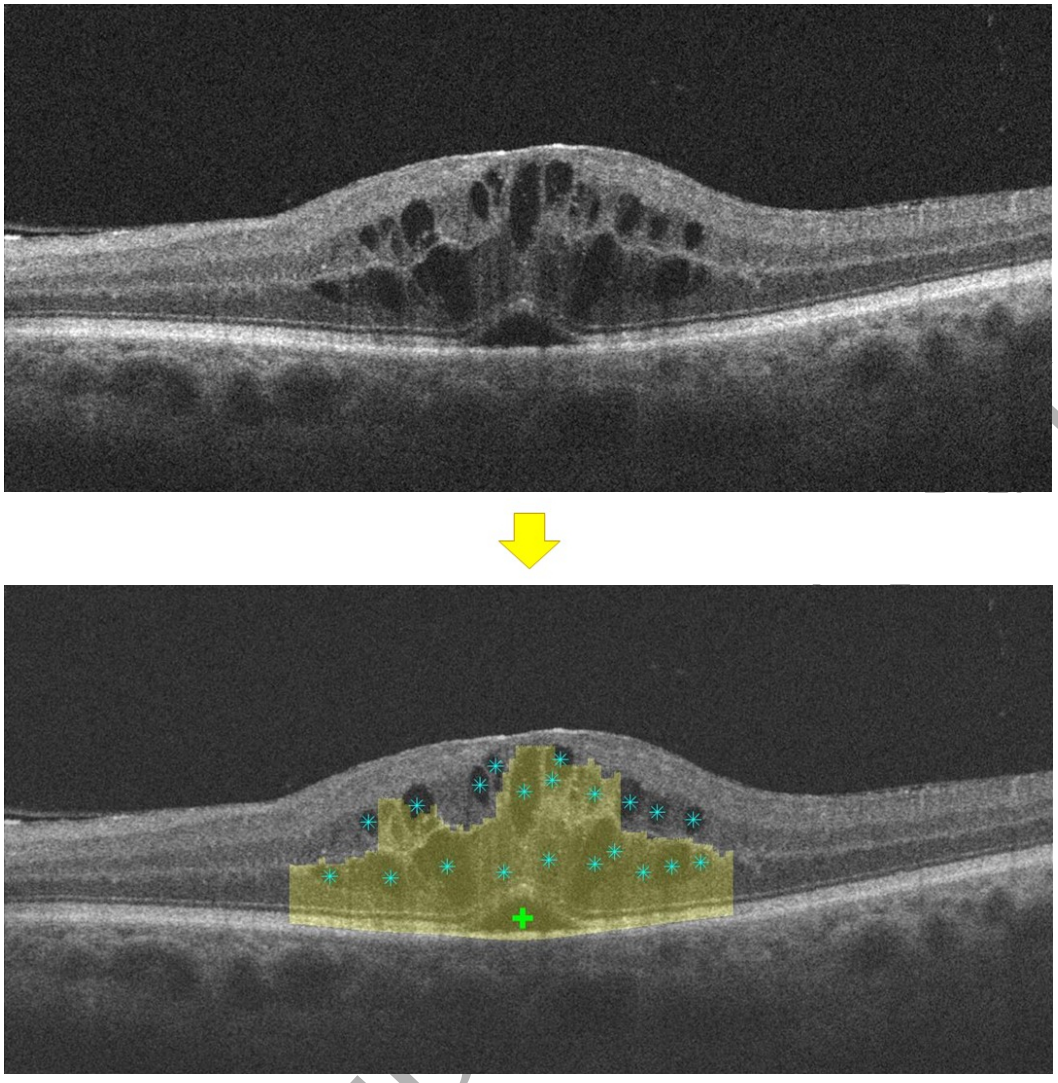

Fig. 19. Example of OCT image with the detection of the three types of MEs: SRD illustrated as (+), CME as (*) and DRT.

Table 7 lists a comparative analysis between two reference works of the literature that faced the CME detection and our proposed strategy. This comparison presents some limitations, given that each proposal used specific private datasets, without any specifications about the selected cases that were used in the study, limiting the comparison among the different analyzed approaches. As we can see, our method shows a competitive performance respect to other proposals.

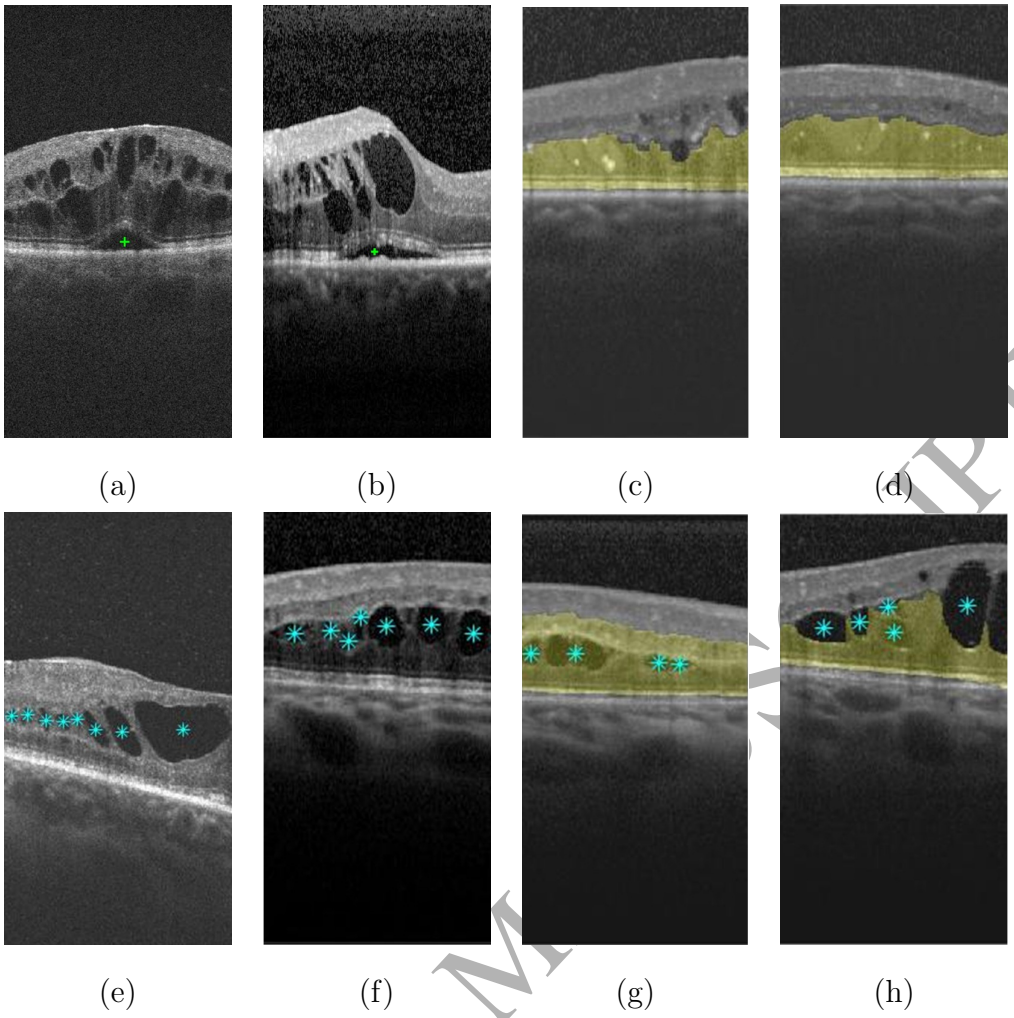

Fig. 20. Examples of ME detection in OCT images: (a) & (b) SRD identification (+). (c) & (d) DRT regional identification. (e) & (f) CME detections (*). (g) & (h) Simultaneous identification of CMEs (*) and DRT.

Table 7
CME detection performance comparison of state-of-the-art approaches and the proposed method.

| **Method** | **Precision** | **Recall** | **F-Measure** |
|---|---|---|---|
| Schlegl *et al.* [18] | 99.00% | 89.00% | 93.73% |
| González *et al.* [21] | 80.00% | 77.11% | 78.53% |
| Proposed | 90.13% | 93.93% | 91.99% |

## 5 Conclusions

In this paper, we propose a complete methodology for the analysis and characterization of the ME presence. This fully automatic system detects and characterizes the three types of ME that may appear in the eye fundus of the patients using OCT images. The OCT scans provide an optimal visualization of the internal characteristics of the retinal layers. Using this information, image processing techniques were combined with learning strategies and complemented with clinical knowledge to build a robust system that accurately aimed to the three types of ME. Regarding their typical pathophysiology, we identified the existing edemas of each ME type, representing useful information for the characterization of the ME disease using the international clinical reference guides.

Regarding the SRD and CME types, both are characterized by a significant drop of intensities combined with their typical morphological shapes as well as the relative position where they normally appear within the retina. Specific adaptive thresholding approaches were applied to identify each type. CMEs are identified with adapted approaches in the inner and outer retina, whereas SRD edemas are searched in the outer retina near the photoreceptors layer. Both identification processes were complemented with expert criterions to remove false candidate detections and obtain a more precise system. In the DRT case, a learning strategy was implemented, testing two representative classifiers as Naive Bayes and SVM to identify columns of the OPL/ISOS region with the DRT presence. This learning approach is more suitable with this type of edemas as they neither present a well-defined boundary nor a significant contrast with the surrounded tissue, presenting a diffuse and regional appear-

ance. To solve this issue, both classifiers where trained and tested to identify these regions using a complete and heterogeneous set of 18 features including intensity, texture and domain knowledge properties. Three feature selectors were applied in this study: RFS, SVM-FS and SFS. The main selected features were taken from the intensity image analysis, mask thickness and GLCM texture-based descriptors. Given that, the best configuration results were obtained from the Naive Bayes classifier and the RFS using the testing dataset. The experimental results show that the proposed system offers a satisfactory performance in the identification and characterization of the ME disease, even when the different types appear combined on the same retinal region. In the case of CMEs, the system achieves a global F-Measure of 91.99% for both retinal regions, while the identification of the DRT presence reaches a value of 87.54%. In the case of the SRD edemas, the system was capable to adequately detect all the cases that appear in the used dataset. Summarizing, despite the high variability and complexity of this retinal pathology, the proposed system is capable to accurately identify all the types of ME, being a useful auxiliary tool to aid the clinicians in the complex and exhausting task of detection and characterization of a relevant disease as is the ME.

Future works include the extension of the methodology with more sophisticated procedures, especially in the case of CMEs in the outer retina, as well as the inclusion of further features and classifiers for the DRT detection. Also, the methodology is planned to be expanded with an automatic detection of MME, providing further medical information for the early diagnosis of ME. To cover the entire characterization of the ME disease, we aim to extend the proposed methodology by its precise segmentation. In addition, further validations could be implemented by the increase of the dataset dimensionality, which enables also the application of other ambitions techniques in this prob-

lematic, as deep learning strategies. Therefore, it will be possible to follow more precisely the evolution of the disease and, consequently, improve the life quality of the patients.

## Acknowledgements

This work is supported by the Instituto de Salud Carlos III, Government of Spain and FEDER funds of the European Union through the PI14/02161 and the DTS15/00153 research projects and by the Ministerio de Economía y Competitividad, Government of Spain through the DPI2015-69948-R research project. Also, this work has received financial support from the European Union (European Regional Development Fund - ERDF) and the Xunta de Galicia, Centro singular de investigación de Galicia accreditation 2016-2019, Ref. ED431G/01; and Grupos de Referencia Competitiva, Ref. ED431C 2016-047.

## References

[1] W. H. Organization, Global Data on Visual Impairments 2010, Geneva: World Health Organ.

[2] R. Bourne, S. Flaxman, T. Braithwaite, M. Cicinelli, A. Das, J. Jonas, J. Keeffe, J. Kempen, J. Leasher, H. Limburg, et al., Magnitude, Temporal Trends, and Projections of the Global Prevalence of Blindness and Distance and Near Vision Impairment: A Systematic Review and Meta-Analysis, The Lancet Global Health 5 (9) (2017) e888–e897.

[3] J. Gass, E. Norton, Cystoid Macular Edema and Papilledema Following

Cataract Extraction: A Fluorescein Fundoscopic and Angiographic Study, Archives of Ophthalmology 76 (5) (1966) 646–661.

[4] A. Joussen, T. Gardner, B. Kirchhof, S. Ryan, Retinal Vascular Disease, Springer Science & Business Media, 2010.

[5] T. Otani, S. Kishi, Y. Maruyama, Patterns of Diabetic Macular Edema with Optical Coherence Tomography, American Journal of Ophthalmology 127 (6) (1999) 688–693.

[6] G. Panozzo, B. Parolini, E. Gusson, A. Mercanti, S. Pinackatt, G. Bertoldo, S. Pignatto, Diabetic Macular Edema: An OCT-Based Classification, in: Seminars in Ophthalmology, Vol. 19, Taylor & Francis, 2004, pp. 13–20.

[7] S. Baamonde, J. de Moura, J. Novo, M. Ortega, Automatic Detection of Epiretinal Membrane in OCT Images by Means of Local Luminosity Patterns, in: International Work-Conference on Artificial Neural Networks, 2017, pp. 222–235.

[8] G. Trichonas, P. K. Kaiser, Optical Coherence Tomography Imaging of Macular Oedema, British Journal of Ophthalmology 98 (Suppl 2) (2014) ii24–ii29.

[9] K. H. Seo, S.-Y. Yu, M. Kim, H. W. Kwak, Visual and Morphologic Outcomes of Intravitreal Ranibizumab for Diabetic Macular Edema Based on Optical Coherence Tomography Patterns, Retina 36 (3) (2016) 588–595.

[10] H. Bogunovic, M. D. Abramoff, L. Zhang, M. Sonka, Prediction of Treatment Response from Retinal OCT in Patients with Exudative Age-Related Macular Degeneration, Proceedings of the Opthalmic Medical Image Analysis First International Workshop.

[11] D. Sidibé, S. Sankar, G. Lemaître, M. Rastgoo, J. Massich, C. Cheung, G. Tan, Milea, et al., An Anomaly Detection Approach for the Identification of DME Patients Using Spectral Domain Optical Coherence Tomography Images, Computer Methods and Programs in Biomedicine 139 (2017) 109–117.

[12] A. Montuoro, S. Waldstein, B. Gerendas, U. Schmidt-Erfurth, H. Bogunović, Joint Retinal Layer and Fluid Segmentation in OCT Scans of Eyes with Severe Macular Edema Using Unsupervised Representation and Auto-Context, Biomedical Optics Express 8 (3) (2017) 1874–1888.

[13] K. Alsaih, G. Lemaitre, M. Rastgoo, J. Massich, D. Sidibé, F. Meriaudeau, Machine Learning Techniques for Diabetic Macular Edema (DME) Classification on SD-OCT Images, Biomedical Engineering Online 16 (1) (2017) 68.

[14] D. Lu, M. Heisler, S. Lee, G. Ding, M. Sarunic, M. Beg, Retinal Fluid Segmentation and Detection in Optical Coherence Tomography Images Using Fully Convolutional Neural Network, CoRR 1710.04778.

[15] C. S. Lee, A. J. Tyring, N. P. Deruyter, Y. Wu, A. Rokem, A. Y. Lee, Deep-Learning Based, Automated Segmentation of Macular Edema in Optical Coherence Tomography, Biomedical Optics Express 8 (7) (2017) 3440–3448.

[16] K. Gopinath, J. Sivaswamy, Segmentation of Retinal Cysts from Optical Coherence Tomography Volumes Via Selective Enhancement, IEEE Journal of Biomedical and Health Informatics.

[17] A. Roy, S. Conjeti, S. Phani Karri, D. Sheet, A. Katouzian, C. Wachinger, N. Navab, Relaynet: Retinal Layer and Fluid Segmentation of Macular Optical Coherence Tomography Using Fully Convolutional Network, Biomedical optics express 8 (8) (2017) 3627–3642.

[18] T. Schlegl, S. Waldstein, H. Bogunovic, F. Endstraßer, A. Sadeghipour, A.-M. Philip, D. Podkowinski, B. S. Gerendas, G. Langs, U. Schmidt-Erfurth, Fully Automated Detection and Quantification of Macular Fluid in OCT Using Deep Learning, Ophthalmology.

[19] G. Girish, B. Thakur, S. R. Chowdhury, A. Kothari, J. Rajan, Segmentation of Intra-Retinal Cysts from Optical Coherence Tomography Images Using a Fully

Convolutional Neural Network Model, IEEE Journal of Biomedical and Health Informatics.

[20] A. Rashno, D. D. Koozekanani, P. M. Drayna, B. Nazari, S. Sadri, H. Rabbani, K. K. Parhi, Fully-Automated Segmentation of Fluid/Cyst Regions in Optical Coherence Tomography Images with Diabetic Macular Edema Using Neutrosophic Sets and Graph Algorithms, IEEE Transactions on Biomedical Engineering.

[21] A. González, B. Remeseiro, M. Ortega, M. Penedo, P. Charlón, Automatic Cyst Detection in OCT Retinal Images Combining Region Flooding and Texture Analysis, in: Computer-Based Medical Systems (CBMS), 2013 IEEE 26th International Symposium on, IEEE, 2013, pp. 397–400.

[22] J. de Moura, J. Novo, J. Rouco, M. Penedo, M. Ortega, Automatic Identification of Intraretinal Cystoid Regions in Optical Coherence Tomography, in: Conference on Artificial Intelligence in Medicine in Europe, Springer, 2017, pp. 305–315.

[23] G. Girish, V. Anima, A. Kothari, P. Sudeep, S. Roychowdhury, J. Rajan, A Benchmark Study of Automated Intra-Retinal Cyst Segmentation Algorithms Using Optical Coherence Tomography B-Scans, Computer Methods and Programs in Biomedicine 153 (2018) 105–114.

[24] M. Esmaeili, A. M. Dehnavi, H. Rabbani, F. Hajizadeh, Three-Dimensional Segmentation of Retinal Cysts from Spectral-Domain Optical Coherence Tomography Images by the Use of Three-Dimensional Curvelet Based K-SVD, Journal of Medical Signals and Sensors 6 (3) (2016) 166.

[25] M. Aharon, M. Elad, A. Bruckstein, $K$-SVD: An Algorithm for Designing Overcomplete Dictionaries for Sparse Representation, IEEE Transactions on Signal Processing 54 (11) (2006) 4311–4322.

[26] J. Starck, E. J. Candès, D. L. Donoho, The Curvelet Transform for Image Denoising, IEEE Transactions on Image Processing 11 (6) (2002) 670–684.

[27] M. Wu, W. Fan, Q. Chen, Z. Du, X. Li, S. Yuan, H. Park, Three-Dimensional Continuous Max Flow Optimization-Based Serous Retinal Detachment Segmentation in SD-OCT for Central Serous Chorioretinopathy, Biomedical Optics Express 8 (9) (2017) 4257–4274.

[28] Z. Sun, H. Chen, F. Shi, L. Wang, W. Zhu, D. Xiang, C. Yan, L. Li, X. Chen, An Automated Framework for 3D Serous Pigment Epithelium Detachment Segmentation in SD-OCT Images, Scientific Reports 6.

[29] M. Bashkansky, J. Reintjes, Statistics and Reduction of Speckle in Optical Coherence Tomography, Optics Letters 25 (8) (2000) 545–547.

[30] G. Samagaio, J. de Moura, J. Novo, M. Ortega, Optical Coherence Tomography Denoising by Means of a Fourier Butterworth Filter-Based Approach, in: International Conference on Image Analysis and Processing, Springer, 2017, pp. 422–432.

[31] S. Chiu, X. Li, P. Nicholas, C. Toth, J. Izatt, S. Farsiu, Automatic Segmentation of Seven Retinal Layers in SDOCT Images Congruent with Expert Manual Segmentation, Opt Express 18 (18) (2010) 19413–19428.

[32] E. Dijkstra, A Note on Two Problems in Connexion with Graphs, Numerische Mathematik 1 (1) (1959) 269.

[33] R. Das, G. Spence, R. Hogg, M. Stevenson, U. Chakravarthy, Disorganization of Inner Retina and Outer Retinal Morphology in Diabetic Macular Edema, JAMA Ophthalmology.

[34] S. Zhu, A. Yuille, Region Competition: Unifying Snakes, Region Growing, and Bayes/MDL for Multiband Image Segmentation, IEEE Transactions on Pattern Analysis and Machine Intelligence 18 (9) (1996) 884–900.

[35] J. Gelfand, R. Nolan, D. Schwartz, J. Graves, A. Green, Microcystic Macular Oedema in Multiple Sclerosis is Associated with Disease Severity, Brain 135 (6) (2012) 1786–1793.

[36] N. Otsu, A Threshold Selection Method from Gray-Level Histograms, IEEE Transactions on Systems, Man, and Cybernetics 9 (1) (1979) 62–66.

[37] H. Noma, H. Funatsu, T. Mimura, K. Shimada, Visual Function and Serous Retinal Detachment in Patients with Branch Retinal Vein Occlusion and Macular Edema: A Case Series, BMC Ophthalmology 11 (1) (2011) 29.

[38] A. Gupta, R. Raman, K. Mohana, V. Kulothungan, T. Sharma, Communications Between Intraretinal and Subretinal Space on Optical Coherence Tomography of Neurosensory Retinal Detachment in Diabetic Macular Edema, Oman Journal of Ophthalmololy 6 (3) (2013) 183.

[39] L. Carmona, F. Hernández, Revisión Bibliográfica: Edema Macular Diabético, Repercusiones y Tratamiento, Revista Médica del Instituto Mexicano del Seguro Social 53 (5) (2015) 600–607.

[40] B. Wolff, G. Azar, V. Vasseur, J.-A. Sahel, C. Vignal, M. Mauget-Faÿsse, Microcystic Changes in the Retinal Internal Nuclear Layer Associated with Optic Atrophy: A Prospective Study, Journal of Ophthalmology 2014 (2014) 3951–3989.

[41] S. Ooto, A. Tsujikawa, S. Mori, H. Tamura, K. Yamashiro, N. Yoshimura, Thickness of Photoreceptor Layers in Polypoidal Choroidal Vasculopathy and Central Serous Chorioretinopathy, Graefe's Archive for Clinical and Experimental Ophthalmology 248 (8) (2010) 1077–1086.

[42] W. Goebel, T. Kretzchmar-Gross, Retinal Thickness in Diabetic Retinopathy: A Study Using Optical Coherence Tomography (OCT), Retina 22 (6) (2002) 759–767.

[43] R. M. Haralick, K. Shanmugam, et al., Textural Features for Image Classification, IEEE Transactions on Systems, Man, and Cybernetics (6) (1973) 610–621.

[44] W. Siedlecki, J. Sklansky, On Automatic Feature Selection, International Journal of Pattern Recognition and Artificial Intelligence 2 (02) (1988) 197–220.

[45] F. Nie, H. Huang, X. Cai, C. Ding, Efficient and Robust Feature Selection Via Joint $\ell 2$, 1-norms Minimization, in: Advances in Neural Information Processing Systems, 2010, pp. 1813–1821.

[46] J. Bi, K. Bennett, M. Embrechts, C. Breneman, M. Song, Dimensionality Reduction Via Sparse Support Vector Machines, Journal of Machine Learning Research 3 (Mar) (2003) 1229–1243.

[47] I. Guyon, A. Elisseeff, An Introduction to Variable and Feature Selection, Journal of Machine Learning Research 3 (Mar) (2003) 1157–1182.

[48] N. Friedman, D. Geiger, M. Goldszmidt, Bayesian Network Classifiers, Machine learning 29 (2-3) (1997) 131–163.

[49] S. S. Keerthi, S. K. Shevade, C. Bhattacharyya, K. R. K. Murthy, Improvements to Platt's SMO Algorithm for SVM Classifier Design, Neural Computation 13 (3) (2001) 637–649.

[50] J. de Moura, J. Novo, P. Charlón, N. Barreira, M. Ortega, Enhanced Visualization of the Retinal Vasculature Using Depth Information in OCT, Medical & Biological Engineering & Computing (2017) 1–17.

[51] H. K. Hahn, H.-O. Peitgen, Iwt-Interactive Watershed Transform: A Hierarchical Method for Efficient Interactive and Automated Segmentation of Multidimensional Gray-Scale Images, in: Proceedings of SPIE, Vol. 5032, 2003, pp. 643–653.

[52] Y. Helmy, H. Allah, Optical Coherence Tomography Classification of Diabetic Cystoid Macular Edema, Clinical Ophthalmology 7 (2013) 1731.

[53] K. Vupparaboina, S. Nizampatnam, J. Chhablani, A. Richhariya, S. Jana, Automated Estimation of Choroidal Thickness Distribution and Volume Based on OCT Images of Posterior Visual Section, Computerized Medical Imaging and Graphics 46 (2015) 315–327.